

Magnetic Damping: Domain Wall Dynamics versus Local Ferromagnetic Resonance

T. Weindler,¹ H. G. Bauer,¹ R. Islinger,¹ B. Boehm,^{1,2} J.-Y. Chauleau,^{1,*} and C. H. Back¹

¹*Department of Physics, Regensburg University, 93040 Regensburg, Germany*

²*IBM Research-Zurich, Säumerstrasse 4, CH-8803 Rüschlikon, Switzerland*

(Received 29 April 2014; published 3 December 2014)

Magnetic relaxation is one of the dominating features of magnetization dynamics. Depending on the magnetic structure and the experimental approach, different magnitudes of the damping parameter are reported even for a given material. In this study, we experimentally address this issue by accessing the damping parameter in the same magnetic nanotracks using different approaches: local ferromagnetic resonance ($\alpha = 0.0072$) and field-driven domain wall dynamics ($\alpha = 0.023$). The experimental results cannot fully be accounted for by modeling only roughness in micromagnetic simulations. Consequently, we have included nonlocal texture induced damping to the micromagnetic code. We find excellent agreement with the observed increased damping in the vortex structures for the same input Gilbert alpha when texture-induced nonlocal damping is included.

DOI: 10.1103/PhysRevLett.113.237204

PACS numbers: 75.78.Fg, 75.40.Gb, 75.60.Ch

Different aspects of magnetization dynamics are involved in magnetic storage technologies based on magnetic domains or on domain wall (DW) dynamics in extended layers and nanostructures [1–6]. Magnetic nanoelements are not only in focus in view of their technological potential but are also often used as test systems for the investigation of debated microscopic mechanisms involved in magnetization dynamics such as, for example, coupling to spin-currents [7–9], heat gradients [10], and the role of spin-orbit coupling in DW dynamics [11,12]. As soon as magnetic textures are dynamically manipulated, one faces dissipation, i.e., the relaxation of excited magnetic textures towards an equilibrium state. Described by Gilbert as a viscous force [13,14], it is modeled as $\alpha \mathbf{m} \times \dot{\mathbf{m}}$, where \mathbf{m} is the local magnetization unit vector, the dot denotes the time derivative, and α the Gilbert damping parameter. In thin ferromagnetic films, the main microscopic mechanism which governs the magnitude of α in absence of defects is dissipation of angular momentum to the lattice via spin-orbit coupling [15,16]. Other established mechanisms that increase the effective damping lie in magnetic inhomogeneities and two magnon scattering [17]. In order to quantitatively access and study complex effects such as current-induced domain wall dynamics, a perfect experimental knowledge of α is required. However, there exists a large spread of reported values even for the prototypical material $\text{Ni}_{80}\text{Fe}_{20}$ depending on details of the experimental method used for its determination. The most common way of evaluating α is to perform ferromagnetic resonance (FMR) experiments. While damping values for $\text{Ni}_{80}\text{Fe}_{20}$ between $\alpha = 0.006$ and $\alpha = 0.008$ are commonly reported by FMR, values needed to interpret DW dynamics range from $\alpha \approx 0.005$ to $\alpha > 0.02$, an issue which has been addressed numerically recently by addressing the role played by roughness [18,19]. Besides, when considering

the dynamics of nonuniform magnetization distributions such as DWs, it has recently been proposed that strong spatial gradients lead to an additional texture-induced nonlocal channel of relaxation [20–22]. While experimental studies of damping in single elliptically shaped nanomagnets [23] and arrays of nanodots [24] have been carried out, no experimental data exist that connect α measured in magnetic racetracks by FMR to α determined using domain wall motion.

In this Letter, we investigate the contribution of texture-induced nonlocal magnetic damping in magnetic racetracks with vortex domain walls. Our experimental approach consists in assessing α in the same nanostructure using two approaches: local FMR and field-driven vortex domain wall dynamics using magneto-optic measurements. On one hand, we use time-resolved scanning Kerr microscopy (TR-MOKE) to perform local FMR on single nanostripes. On the other hand, in exactly the same nanostripes, DWs are injected and field-driven displacements are analyzed by wide-field Kerr microscopy. To undermine our findings, we have included a texture-induced nonlocal damping term in a micromagnetic solver [21] as well as edge and surface roughness. This study aims at lifting the controversy regarding the value of α seemingly depending on the experimental approach. Furthermore, we quantitatively evaluate the contribution of texture-induced nonlocal damping.

The samples under study are $\text{Ni}_{80}\text{Fe}_{20}$ nanostripes of various widths (0.5–1.25 μm) and 20 nm thickness, capped by 3 nm of Al [Fig. 1(a)]. At one extremity, an elliptical nucleation pad is attached while the other one terminates as a tip to favor DW annihilation [Figs. 1(a) and 1(b)]. These magnetic nanostructures are fabricated on top of Au coplanar waveguides used for continuous wave high frequency excitation to perform FMR and for field-driven DW dynamics by connecting either a high frequency generator

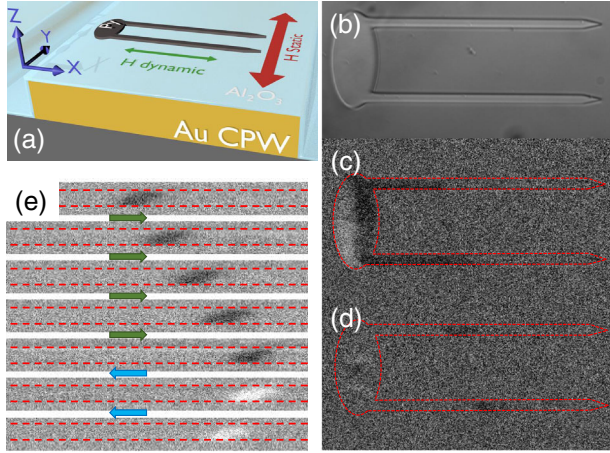


FIG. 1 (color online). Domain wall dynamics observed by wide-field Kerr microscopy. (a) Schematic diagram of the sample layout. (b) Optical image of the magnetic structure. The stripe width is $1 \mu\text{m}$ and the dimension of the ellipse part is $15 \times 7.5 \mu\text{m}^2$. (c) Magnetic contrast after injecting DWs. (d) Magnetic contrast after pushing the DWs of (c) by a second field pulse. Magnetic contrast images are obtained by computing difference images, see Supplemental Material [25]. (e) Series of back and forth displacements of one DW in a $1.2 \mu\text{m}$ wide stripe. Arrows represent the field pulse direction.

or a pulse generator to the 50 Ohm matched devices. This dynamic field is generated along the long axis of the stripe [i.e., x axis, Fig. 1(a)]. Magnetic structures and coplanar waveguides are electrically decoupled by 7 nm of Al_2O_3 .

A standard procedure of image difference (see Supplemental Material [25]) is applied in order to enhance the magnetic contrast. The access to different magnetic states allows us to either detect the DW position [Fig. 1(c)] or the DW displacement [Figs. 1(d) and 1(e)]. Pushed by a magnetic field pulse, DWs move, increasing the size of the domain favored by the field direction. Subsequently, back and forth displacements [Fig. 1(e)] can be analyzed as function of the field pulse magnitude, see Fig. 2(a).

In this study, we analyze the characteristics of the steady-state regime [26] to extract the effective damping:

$$\frac{\delta q}{\Delta_T} = \frac{\gamma}{\alpha} \int \mu_0 H_x(t) dt - \frac{1}{\alpha} \int \frac{d\phi}{dt} dt, \quad (1)$$

where δq is the DW displacement (difference between the final and initial generalized position), ϕ the generalized wall angle [27], Δ_T the Thiele width [28,29], γ the gyromagnetic ratio, μ_0 the vacuum permeability, and $H_x(t)$ the time-dependent magnetic field amplitude along the x axis. The second term on the right-hand side of Eq. (1) has no contribution in the steady-state regime since no DW transformation occurs [27,30] and will be neglected for the fitting procedure. At constant field pulse length, the quantity $\delta q/\Delta_T$ increases linearly as a function of the field amplitude with a slope inversely proportional to α . Note that Eq. (1) is

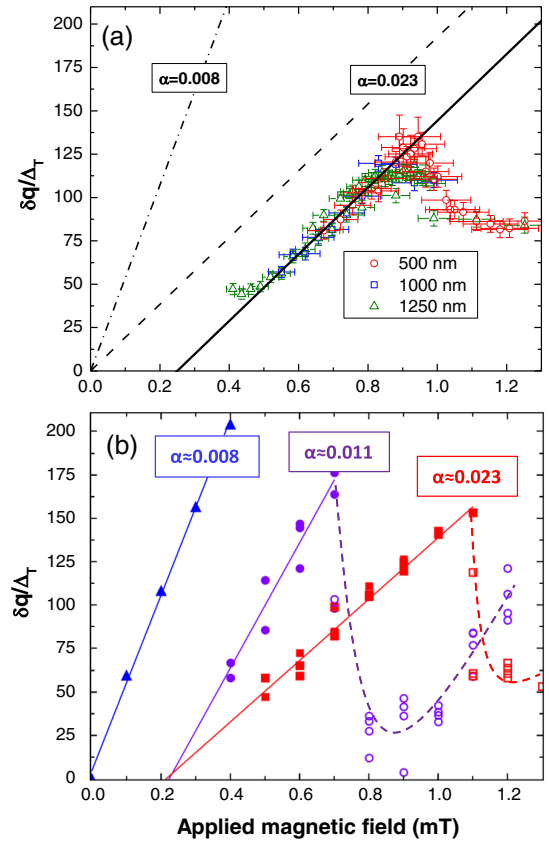


FIG. 2 (color online). (a) Normalized DW displacement ($\delta q/\Delta_T$) as a function of applied magnetic field amplitude for stripes of different widths. The black straight line is a linear fit of DW dynamics in the linear regime. The dashed and dot-dashed lines are the expected behaviors in the steady state regime for $\alpha = 0.023$ and $\alpha = 0.008$. (b) Computed normalized DW displacement as a function of the applied magnetic field amplitude for a 512 wide and 17 nm thick $\text{Ni}_{80}\text{Fe}_{20}$ stripe for a perfect stripe (blue triangles) and with 3.5% surface roughness (purple dots) and with 3.5% surface roughness and texture-induced damping (red squares). Open (filled) symbols stand for DW dynamics above (below) the Walker breakdown.

exact as long as a generalized position and Thiele width are considered [27].

Figure 2(a) presents the quantity $\delta q/\Delta_T$ as a function of the applied field magnitude which allows us to directly compare stripes with different widths. Thiele widths (Δ_T) are computed by micromagnetic simulations and lead to: 28.9, 41.8, and 46.6 nm for 500, 1000, and 1250 nm wide stripes, respectively. Note that Δ_T is not independent of the applied field since the wall structures slightly deform in the steady-state regime. Yet, the deformation is less than 3% and can therefore be neglected. Interestingly, even though DWs have different pinning fields for different stripe widths (≈ 0.62 , 0.55, and 0.43 mT for 500, 1000, and 1250 nm wide stripes, respectively), their normalized dynamics ($\delta q/\Delta_T$) are identical in the steady-state regime.

By fitting the slope of this regime, the effective damping parameter is determined to be $\alpha = 0.023 \pm 0.005$.

The main objective of this study is to compare magnetic damping obtained from field-driven DW dynamics to FMR. This is achieved by performing time-resolved Kerr microscopy on the exact same set of stripes as the ones used for DW dynamics. A static applied magnetic field is swept along the y axis [Fig. 1(a)] while the frequency of the rf field is kept constant. The amplitude of the polar Kerr signal is acquired as a function of the applied static field revealing the different magnetic resonances of the magnetic system [Figs. 3(a) and 3(d)]. The pieces of information extracted at a given frequency are the resonant field $\mu_0 H_0$ and the linewidth $\mu_0 \Delta H$. The finite size of the stripes leads to the presence of nonuniform modes in the spectra. The analysis is therefore performed using a multi-Lorentzian fit. The resonant field as function of excitation frequency is shown in Figs. 3(b) and 3(e) and fitted using Kittel's formula which

is expressed in the case of an extended magnetic layer without anisotropy as $\omega = \mu_0 \gamma \sqrt{H_0(H_0 + M_S)}$ with $\omega = 2\pi f$ the angular frequency and H_0 the resonant field. The gyromagnetic ratio γ plays a non-negligible role in the determination of the damping parameter in both DW dynamics and FMR measurements and is the only fit parameter. The saturation magnetization ($\mu_0 M_S = 0.92$ T) has been measured independently by superconducting quantum interference device measurements on a reference layer. The Kittel equation is exact for a uniform magnetization distribution in an extended layer for which the *ellipse* part of the structure provides a good approximation. However, its finite size leads to higher harmonic modes [31], easily identified by imaging the structure at the respective resonant field for a given excitation frequency [see inset of Fig. 3(b)]. The fit of the main mode results in a gyromagnetic ratio value of $\gamma = 1.88 \pm 0.02 \times 10^{11} \text{ T}^{-1} \text{ s}^{-1}$. Regarding the *stripe* part of the structure, the analysis is more delicate since in order to study the exact same set of structures as the one used for DW dynamics, the stripes are magnetized transversally to their long axis. The analysis is achieved by considering the magnetic system saturated along a uniaxial anisotropy axis. Kittel's formula is thus changed to: $\omega = \mu_0 \gamma \sqrt{(H_0 + H_K)(H_0 + H_K + M_S)}$, where H_K is the uniaxial anisotropy field, also considered as a fit parameter. In this configuration, edge modes [32] are visible at higher fields [see Fig. 3(d)]. Figure 3(e) displays only the main modes for stripes with different widths. Fitting these results provides $\gamma = 1.86 \pm 0.02 \times 10^{11} \text{ T}^{-1} \text{ s}^{-1}$.

Once the gyromagnetic ratio is obtained, the Gilbert damping parameter can be extracted from the analysis of the linewidth ($\mu_0 \Delta H$). Figures 3(c) and 3(f) display $\mu_0 \Delta H$ as a function of the excitation frequency for the main modes of the *ellipse* and *stripe* parts of the structures. In the case of uniform magnetization distributions in an extended magnetic layer, the following relation holds: $\mu_0 \Delta H = \alpha \omega / \gamma$. By linearly fitting the measured linewidths as a function of the excitation frequency [Figs. 3(c) and 3(f)], one obtains values for the intrinsic Gilbert damping parameter α on the *ellipse* part: $\alpha = 0.0079 \pm 0.0003$ and on the *stripe* parts: $\alpha = 0.0072 \pm 0.0007$.

These values are in the range of the ones commonly reported for FMR on full magnetic films and on nanomagnets. However, they are 2.5 times lower than the values extracted from field driven DW dynamic experiments performed on the exact same stripes. In order to stress this difference, we display in Fig. 2(a), the expected behavior of the steady-state regime with $\alpha = 0.008$ and in Fig. 3(f) display the expected frequency dependence of the linewidth ($\mu_0 \Delta H$) for $\alpha = 0.023$. One can clearly note the discrepancy with respect to the measured data.

Interestingly, no size-dependent effect can be noticed. Similarly to the quantity $\delta q / \Delta_T$ extracted from the field-driven DW dynamics experiments, the frequency-dependence

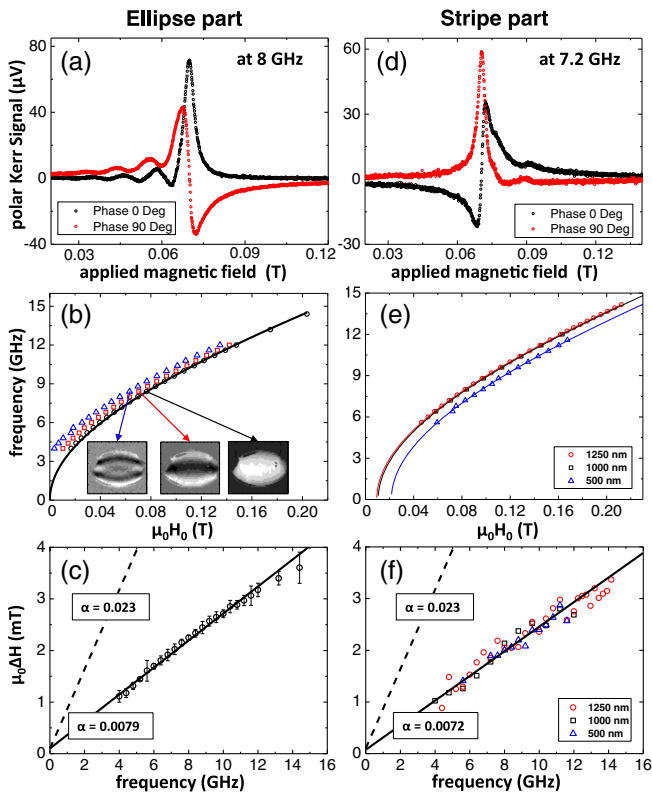


FIG. 3 (color online). Local FMR analysis of the nanostructures. Resonance spectra on the *ellipse* (a) and *stripe* (d) parts of the structure. Dependence of the resonant frequency on the resonant field: (b) measured on the *ellipse* part where the main mode and two harmonics can be evidenced (inset); (e) measured on the *stripe* part for which only the main modes for three different stripe widths are shown. Main modes linewidths for the *ellipse* (c) and *stripe* (f) parts of the structure as function of frequency. The straight black lines represent the linear fit as a function of frequency of $\mu_0 \Delta H$, whereas the dashed black lines represent $\alpha = 0.023$.

of the linewidth does not show any significant dependence on the stripe width. Above all, the facts that i) the extrinsic contribution, i.e., zero frequency offset in Figs. 3(c) and 3(f) is similar for both the *ellipse* and *stripes* parts (≈ 0.1 mT) and that ii) no significant difference for stripes with various widths is observed, exclude a predominant effect of the nanostructuring on the damping.

As discussed in Refs. [18,19], roughness plays a major role in DW dynamics. Figure 2(b) presents a micromagnetic simulation of a vortex DW in a 512 nm wide and 17 nm thick stripe subjected to 23 ns field pulses. The cell size is approximately 5 by 5 by 17 nm. We define the domain wall displacement as the difference between the final and initial position of the vortex core in the domain wall. A value of $\alpha = 0.008$ has been evaluated using Eq. (1) for the perfect wire, which corresponds to the input value for all micromagnetic simulations. From DW dynamics data, pinning fields and nonzero offset (or H_i , see Fig. 2) are two important indicators of roughness. For a perfect stripe, as expected, the two latter are equal to zero. As soon as roughness is implemented, a finite pinning field is reproduced as well as a finite nonzero offset. This can also be understood in the frame of Eq. (1) by a small contribution of the second term due to the reduction of the DW inertia [30,33] by the roughness. Surface roughness is modeled as a variation of the saturation magnetization between 2% and 6% on a length scale of approximately 10 by 10 nm, which mimics thickness variations, see Ref. [18]. The introduction of surface roughness (3.5%) leads to an increase of the effective damping to $\alpha \approx 0.011$ and allows us to fairly well reproduce pinning field and nonzero offset [Fig. 2(b)]. We have additionally tested other ways of modeling disorder (Fig. 4) such as edge roughness which was modeled by removing different parts of the first or

second outermost cells of the magnetic material on each side of the stripe [34,35].

Figure 4 summarizes the extracted relative ratio $\alpha_{\text{input}}/\alpha_{\text{eff}}$ (with $\alpha_{\text{input}} = 0.008$) for a large set of simulations including different types of roughness. The increase of the degree of disorder leads indeed to a reduction of the slope but the dominant effect is the increase of the pinning field and of H_i (Fig. 2) which eventually hides the steady-state regime, clearly inconsistent with the experimental data. In order to emphasize this point, $\alpha_{\text{input}}/\alpha_{\text{eff}}$ is displayed as function of the quantity $[(H_w - H_i)/H_w]$ with H_w the Walker field. Note that in the case of a perfect stripe, $(H_w - H_i)/H_w = 1$ and $\alpha_{\text{input}}/\alpha_{\text{eff}} = 1$.

To explicitly account for the role of conduction electrons in transferring angular momentum away from regions of magnetization varying strongly in space and time, Zhang *et al.* [21] have developed an analytic expression for conducting ferromagnets. The spatially varying time-dependent magnetization generates a nonuniform spin current which carries away the nonequilibrium angular momentum and energy, resulting in the tensorial form of the damping term: $\mathbf{m} \times (\mathcal{D} \cdot \dot{\mathbf{m}})$ with \mathcal{D} , a 3×3 tensor whose elements are the sum of the conventional intrinsic Gilbert damping (α) and a component involving magnetization gradients, weighted by a new material-dependent parameter η as defined in Ref. [21]:

$$\mathcal{D}_{ij} = \alpha \delta_{ij} + \eta \sum_{n=x,y,z} (\mathbf{m} \times \partial_n \mathbf{m})_i (\mathbf{m} \times \partial_n \mathbf{m})_j, \quad (2)$$

with δ_{ij} , the Kronecker symbol. This expression has been included in the micromagnetic code [36].

In Fig. 4, results are shown including ($\eta = 0.07 \text{ nm}^2$) and excluding ($\eta = 0$) texture-induced nonlocal damping. While solely introducing roughness fails reproducing the large increase in damping observed in DW dynamics, a nonzero η clearly allows a DW dynamics similar to experimental observations (pinning field, H_i , and α_{eff}). Note that different thicknesses and M_S have been tested, evidencing that these parameters affect mainly the Walker field and not the effective damping. This strengthens the role played by the texture-induced nonlocal damping.

Our experimental approach has allowed us to independently evaluate the effective damping of DW dynamics, the intrinsic alpha and the role of roughness. Including the nonlocal expression, it becomes possible to reproduce the experimental DW dynamics behavior with a fairly good agreement [Fig. 2(b)] for $\eta = 0.07 \text{ nm}^2$ showing that high spatial gradients located at the vortex core position play a dominant role in DW dynamics.

To conclude, in this study, we have experimentally assessed the damping parameter α on the same set of nanostripes by two complementary approaches: field-driven domain wall dynamics and local ferromagnetic resonance. The effective damping parameter extracted from

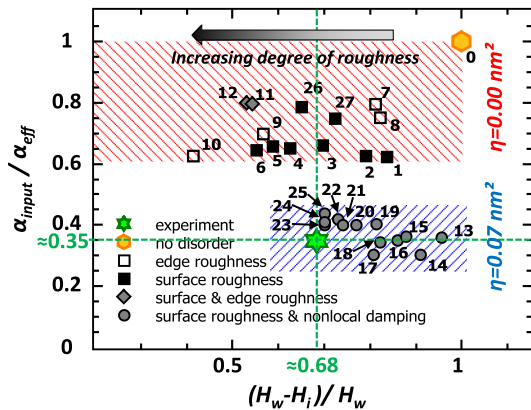


FIG. 4 (color online). Results of the micromagnetic domain wall displacement simulations for a 512 nm wide stripe of $\text{Ni}_{80}\text{Fe}_{20}$. α_{eff} has been obtained from the slope of the linear part of displacement vs field plots up to the Walker breakdown field (H_w), and H_i is the intersect of that straight line with the field axis. α_{input} is 0.008. The different parameters used for each simulation are listed in the Supplemental Material [25].

DW dynamics is about 2.5 times larger than the one measured by local FMR. Even if roughness plays a role in this increase, it can not be the only cause. Therefore, we have been able to assess the texture-induced nonlocal part of the damping by quantitatively determining its weighting parameter in the case of vortex wall dynamics: $\eta \approx 0.07 \text{ nm}^2$.

We thank Dr. R. Schäfer for his advice regarding wide-field magneto-optic imaging. J.-Y.C. wishes to thank the Alexander von Humboldt-Stiftung for financial support. We also acknowledge the DFG for funding via SFB 689. The research leading to these results has received funding from the European Union Seventh Framework Programme (FP7-People-2012-ITN) under Grant No. 316657 (SpinIcur).

*jean-yves.chauleau@cea.fr

- [1] D. A. Allwood, G. Xiong, C. C. Faulkner, D. Atkinson, D. Petit, and R. P. Cowburn, *Science* **309**, 1688 (2005).
- [2] S. A. Wolf, D. D. Awschalom, R. A. Buhrman, J. M. Daughton, S. von Molnár, M. L. Roukes, A. Y. Chtchelkanova, and D. M. Treger, *Science* **294**, 1488 (2001).
- [3] S. Parkin, M. Hayashi, and L. Thomas, *Science* **320**, 190 (2008).
- [4] S. S. P. Parkin, U.S. Patents 6,834,005, 6,898,132, 6,920,062, 7,031,178 and 7,236,386 (2004–2007).
- [5] S. Fukami, T. Suzuki, N. Ohshima, K. Nagahara, and N. Ishiwata, *J. Appl. Phys.* **103**, 07E718 (2008).
- [6] A. Pushp, T. Phung, C. Rettner, B. Hughes, L. Thomas, S.-H. Yang, and S. Parkin, *Nat. Phys.* **9**, 505 (2013).
- [7] G. S. D. Beach, M. Tsoi, and J. L. Erskine, *J. Magn. Mater.* **320**, 1272 (2008).
- [8] T. A. Moore, M. Kläui, L. Heyne, P. Möhrke, D. Backes, J. Rhensius, U. Rüdiger, L. J. Heyderman, J.-U. Thiele, G. Woltersdorf *et al.*, *Phys. Rev. B* **80**, 132403 (2009).
- [9] S. Lepadatu, J. S. Claydon, C. J. Kinane, T. R. Charlton, S. Langridge, A. Potenza, S. S. Dhesi, P. S. Keatley, R. J. Hicken, B. J. Hickey *et al.*, *Phys. Rev. B* **81**, 020413 (2010).
- [10] G. E. W. Bauer, S. Bretzel, A. Brataas, and Y. Tserkovnyak, *Phys. Rev. B* **81**, 024427 (2010).
- [11] K.-S. Ryu, L. Thomas, S.-H. Yang, and S. Parkin, *Nat. Nanotechnol.* **8**, 527 (2013).
- [12] O. Boulle, S. Rohart, L. D. Buda-Prejbeanu, E. Jue, I. M. Miron, S. Pizzini, J. Vogel, G. Gaudin, and A. Thiaville, *Phys. Rev. Lett.* **111**, 217203 (2013).
- [13] T. Gilbert, Ph.D. thesis, Illinois Institute of Technology, Chicago, 1956.
- [14] T. Gilbert, *IEEE Trans. Magn.* **40**, 3443 (2004).
- [15] V. Kambersky, *Czech. J. Phys. B* **26**, 1366 (1976).
- [16] K. Gilmore, Y. U. Idzerda, and M. D. Stiles, *Phys. Rev. Lett.* **99**, 027204 (2007).
- [17] K. Zakeri, J. Lindner, I. Barsukov, R. Meckenstock, M. Farle, U. von Hörsten, H. Wende, W. Keune, J. Rucker, S. S. Kalarickal *et al.*, *Phys. Rev. B* **76**, 104416 (2007).
- [18] H. Min, R. D. McMichael, M. J. Donahue, J. Miltat, and M. D. Stiles, *Phys. Rev. Lett.* **104**, 217201 (2010).
- [19] B. Van de Wiele, L. Laurson, and G. Durin, *Eur. Phys. J. B* **86**, 86 (2013).
- [20] J. Foros, A. Brataas, Y. Tserkovnyak, and G. E. W. Bauer, *Phys. Rev. B* **78**, 140402(R) (2008).
- [21] S. Zhang and Steven S.-L. Zhang, *Phys. Rev. Lett.* **102**, 086601 (2009).
- [22] Z. Yuan, K. Hals, Y. Liu, A. Starikov, A. Brataas, and P. Kelly, [arXiv:1404.1488](https://arxiv.org/abs/1404.1488).
- [23] H. T. Nembach, J. M. Shaw, C. T. Boone, and T. J. Silva, *Phys. Rev. Lett.* **110**, 117201 (2013).
- [24] J. M. Shaw, T. J. Silva, M. L. Schneider, and R. D. McMichael, *Phys. Rev. B* **79**, 184404 (2009).
- [25] See Supplemental Material at <http://link.aps.org/supplemental/10.1103/PhysRevLett.113.237204> for technical descriptions of domain wall dynamics assessed by wide-field Kerr microscopy and of local ferromagnetic resonance assessed by time-resolved Kerr microscopy. A last part is dedicated to the parameters used for the micromagnetic simulations.
- [26] N. Schryer and L. Walker, *J. Appl. Phys.* **45**, 5406 (1974).
- [27] A. Thiaville, Y. Nakatani, F. Piéchon, J. Miltat, and T. Ono, *Eur. Phys. J. B* **60**, 15 (2007).
- [28] A. Thiele, *J. Appl. Phys.* **45**, 377 (1974).
- [29] Y. Nakatani, A. Thiaville, and J. Miltat, *J. Magn. Mater.* **290–291**, 750 (2005).
- [30] J.-Y. Chauleau, R. Weil, A. Thiaville, and J. Miltat, *Phys. Rev. B* **82**, 214414 (2010).
- [31] I. Neudecker, K. Perzlmaier, F. Hoffmann, G. Woltersdorf, M. Buess, D. Weiss, and C. H. Back, *Phys. Rev. B* **73**, 134426 (2006).
- [32] J. P. Park, P. Eames, D. M. Engebretson, J. Berezovsky, and P. A. Crowell, *Phys. Rev. Lett.* **89**, 277201 (2002).
- [33] L. Thomas, R. Moriya, C. Rettner, and S. S. Parkin, *Science* **330**, 1810 (2010).
- [34] Y. Nakatani, A. Thiaville, and J. Miltat, *Nat. Mater.* **2**, 521 (2003).
- [35] C. Zinoni, A. Vanhaverbeke, P. Eib, G. Salis, and R. Allenspach, *Phys. Rev. Lett.* **107**, 207204 (2011).
- [36] A. Vansteenkiste and B. Van de Wiele, *J. Magn. Mater.* **323**, 2585 (2011).